Communauté
UNIVERSITÉ Grenoble Alpes

RAPPORT DE MÉMOIRE DE FIN D'ÉTUDES

Pour l'obtention du:

DIPLOME DE MASTER EEA

Spécialité : **Systems, Control and Information Technologies (MiSCIT)**

Présenté par

Hamza MAMECHE

Stage encadrée par **E. WITRANT**
et co-encadrée par **C. PRIEUR**

effectué au sein de **GIPSA-lab**

Control of electron temperature profile in H-mode tokamak plasmas

Mémoire soutenu publiquement le **19 Juin 2018**,
devant le jury composé de :

G. BESANÇON
Professeur Grenoble-INP, Président
F. FERRANTE
Maître de conférences UGA, Rapporteur
E. WITRANT
Maître de conférences UGA, Encadrant du stage
C. PRIEUR
Directeur de Recherche CNRS, Co-encadrant du stage

Abstract

This work is dedicated to the stability and to control of the electron temperature profile in H-mode tokamak plasmas, Lyapunov stability analysis is carried in an infinite-dimensional setting on the nonlinear partial differential equation describing the dynamics. The nonlinear components are handled with the sum of squares framework, to prove the asymptotic convergence of the Lyapunov function. A profile tracking control of the electron temperature is done using a PI controller, and simulations are performed on the RAPTOR simulator with different challenging scenarios.

Résumé

Ce travail a été consacré à la stabilité et au contrôle du profil de la température des électrons dans les plasmas de tokamak dans le cas des plasmas à confinement élevé, en employant la méthode de Lyapunov pour la stabilité des systèmes à dimension infini sur l'equation différentielle partielle non linéaire qui décrit les dynamiques du système. Vue la non-linéarité du système, on utilise l'approche de la somme des carrés pour prouver la convergence asymptotique de la fonction de Lyapunov, part la suite, un contrôleur de type PI a été utilisé pour le suivi de profil, et a été testé sur le simulateur RAPTOR avec des scénarios stimulants.

Contents

Chapter 1

Introduction

With the world's population growth of 1% a year and more importantly the economic growth of 3.3% a year, the world energy consumption is estimated to increase by 28% from 2015 to 2040 [2]. In addition, oil and gas which represent 57% of the world energy consumption in 2015, have a current R/P ratio [1] of around 52 years [1]. In this context comes the necessity of reducing the dependency on the fossil fuel and relying on renewable energy sources such as solar and wind power, or on the nuclear energy. Knowing that renewable energy sources have low energy density, and taking into account the danger that comes from the nuclear fission energy plants, makes the nuclear fusion a promising option to adopt as part of the solution to the energy problem. This is justified since it has a very high energy density, practically inexhaustible fuels, no greenhouse emissions and the only waste of a fusion plant is the ferritic steel (used as the structure material of the fusion pant) activated by the neutrons whose radioactivity quickly converge to the level of coal ash within few hundreds of years. In addition to that, the fusion plant operates with near 1 g of fuel in reaction, also the impossibility of chain reaction occurrence presents no risk for catastrophic accident.

1.1 Thermonuclear Fusion

Nuclear fusion energy is based on the energy released when two light nuclei fuse to form a heavier nucleus. In order for that to happen, the nuclei must overcome the coulomb barrier to get close enough where the strong nuclear force can operate and fuse them. To overcome the coulomb barrier, the plasma containing the nuclei should

[1] The Reserves-to-production ratio is the remaining amount of a non-renewable resource, expressed in time

be hot enough. Based on the reaction rate $\langle \sigma v \rangle$, the Deuterium-Tritium reaction (1.1) is the most promising one since it reaches a peak value of the reaction rate at a relatively low energy of 10 keV.

$$ {}^{2}_{1}\mathrm{D} + {}^{3}_{1}\mathrm{T} \longrightarrow {}^{4}_{2}\mathrm{He}(\,3.5\,\mathrm{Mev}) + {}^{1}_{0}\mathrm{n}(\,14.1\,\mathrm{Mev}) \tag{1.1} $$

The energy is released in the form of kinetic energy with an outcome of $E_{released} = 17.6$ MeV. As for the incomes, the Deuterium ${}^{2}_{1}\mathrm{D}$ is very abundant on earth, while the tritium ${}^{3}_{1}\mathrm{T}$ has to be bred from lithium ${}^{6}\mathrm{Li}$ which is also abundant using the neutrons produced by (1.1) as :

$$ {}^{6}\mathrm{Li} + \mathrm{n} \longrightarrow 2\,{}^{4}_{2}\mathrm{He} + {}^{3}_{1}\mathrm{T} \tag{1.2} $$

The fusion plant needs energy in terms of heating and current drive sources to reach and maintain the fusion, and produce electricity from the heating of the blankets surrounding the machine with the resulting neutrons. To reach the break-even, the produced heating energy should surpass the energy used to maintain the fusion. For that to happen the plasma must satisfy :

$$ n_e \tau_E \geq \frac{2T}{\langle \sigma v \rangle E_\alpha} \tag{1.3} $$

where n_e is the electron density, T is the plasma temperature, E_α is the energy of the α-particles released during the fusion reactions, and τ_E is the energy confinement time, which can be written as $\tau_E = W/P_{loss}$ where W is the plasma energetic content and P_{loss} the lost power . Furthermore, to reach ignition, where the plasma is self-sustained, which means that the heating produced from the collisions of the α-particles maintain the fusion reaction, for that to happen, we must have:

$$ n_e \tau_E|_{ignition} \geq 6\; n_e \tau_E|_{Break-even} \tag{1.4} $$

1.2 Magnetic confinement and tokamaks

While the plasma in the sun is confined using its huge gravitational field, earth made plasma relies on different ways to be confined, one of these approaches is the magnetic confinement. In toroidal magnetic confinement, the plasma is confined in a torus using the fact that charged particles rotate around magnetic field lines. This toroidal magnetic field is generated by a set of coils, which means that its strength decays when moving away from the symmetry axis. A gradient in the magnetic field is

thus created and gives birth to a gradient drift in the plasma. This drift is charge dependent, which means that charged particles drift in different directions based on their charges which then creates a charge independent outward $\overrightarrow{E} \times \overrightarrow{B}$ drift driving the plasma to the walls, since no material will stand with 10 keV plasma we should twist the magnetic field lines either by twisting the coils structure in the **stellarator** solution case, or by adding a poloidal magnetic field generated this time by an induced plasma current in the **tokamak** solution case.

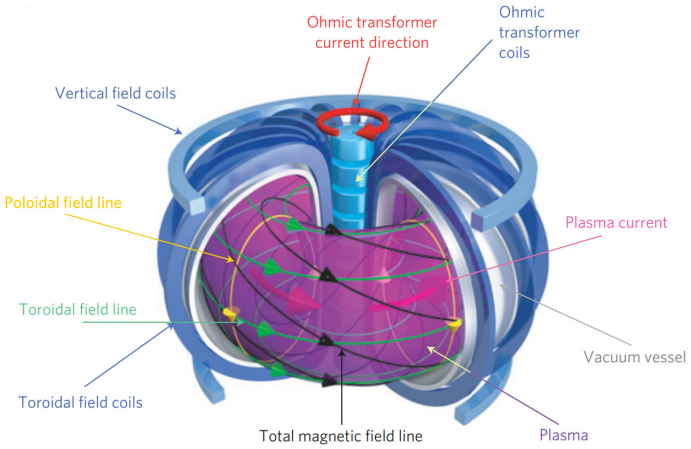

Figure 1.1: Representation of a tokamak configuration (from [19])

Focusing on the tokamak solution, we see in Figure 1.1 the configuration of a typical tokamak. The induced plasma current heats the plasma but up to a limit since the resistivity of the plasma decay with temperature, to further heat the plasma we use auxiliary heating sources like : Natural Beam Injection (NBI) which heats the plasma by the collisions made by the injected accelerated neutral atoms; or by injecting electromagnetic waves that resonate with the plasma particles and dispose its energy to heat the plasma in the case of Ion Cyclotron Resonance Heating (ICRH) and Electron Cyclotron Resonance Heating (ECRH); or to drive a non-inductive current with Ion Cyclotron Current Drive (ICCD) and Electron Cyclotron Current Drive (ECCD). These auxiliary heating and current drive sources give a degree of freedom to shape and control the plasma because of their local disposition.

1.3 Control problems in tokamaks

The overall objective of controlling the plasma is to steer it towards a desired operation point defining a plasma scenario, a baseline for high-performance scenario for

tokamaks is H-mode (High confinement mode), where the plasma is heated strongly exceeding a threshold to a point that the transport of plasma energy in the edge area is reduced forming a transport barrier. In this mode, the energy confinement time is significantly enhanced, typically by a factor of 2 or more [13]. To reach and maintain these high-performance scenarios, **plasma profiles control** plays a fundamental role. These profiles are grouped as: Magnetic radial profiles such as poloidal magnetic flux $\Psi(x)$ and the safety factor $q(x)$ or its inverse $\iota(x)$; and kinetic profiles such as electron and ion temperature and density. These are spatially distributed profiles with two-time scales coupled nonlinear dynamics, hence the difficulty of the control problem. Different approaches have been made to tackle these difficulties. In [16] and [17] a two-time scale linearized data-driven model was built based on singular perturbations theory, and was used to control the poloidal magnetic flux $\Psi(x)$ and the safety factor $q(x)$ in [18]. Other works used first-principles-driven models that capture the dominant and relevant dynamics to synthesize the controller as in [26] [9]. Taking into account the spatially distributed nature of the dynamics, [4] used a spatially discretized model for current profile control, where other works used infinite dimensional theory to synthesize the control algorithms as in [3].

While some works emphasized on the coupling between the dynamics and used a linearized model [15], we are interested in the nonlinearity of the dynamics. In this scope, control of nonlinear PDEs is a recent and challenging topic. An interesting way to tackle the problem is to separate a "slow" finite set of eigenvalues of the system operator that capture the dominant dynamics, and use it as a basis for synthesizing the finite-dimensional controller [6]. But in the case of nonlinear parabolic PDEs, a precise approximation of the dynamics may leads to a large number of modes that should be included [5], and this is what motivates us to choose the infinite-dimensional control theory to tackle the problem. As in [11], we choose to use a proportional-integral control so that the stability of the closed loop system is guaranteed. The goal of this work is to develop, using infinite dimensional control theory, a control algorithm for the electron temperature profile T_e. For that we use a simplified nonlinear diffusion PDE of the electron temperature profile and we slightly modify the transport model to incorporate the H-mode pedestal. We apply a PI controller for tracking, then we use the RAPTOR (RApid Plasma Transport simulatOR) simulator [10] to test this control strategy with the TCV (Tokamak à Configuration Variable) tokamak settings.

1.4 Outline of the thesis

This thesis is organized as follows; In Chapter 2, we present the dynamical model for the electron temperature profile including the transport model modification to represent the H-mode pedestal, and the input constraints. In Chapter 3 we recall the direct Lyapunov method for the stability analysis for PDEs, and we use a weighted Lyapunov function to study the stability of the autonomous dynamics. We then use a PI controller as a feedback to control the dynamics and discuss the stability of the closed loop system. Finally, in Chapter 4 we use the RAPTOR simulator to evaluate the control strategy including the input constraints.

Chapter 2

Control-oriented model and objectives

In this chapter, we present the dynamical model for the electron temperature profile, the control inputs and their constraints, and the control objectives we are intended to reach. The main physical variables are summarized in Table 2.1.

2.1 Electron temperature equation

Under the use of infinite cylinder geometry, a hypothesis for the transport to be symmetrical in the toroidal and the poloidal directions [7], the electrons temperature T_e and density n_e dynamics are described by the diffusion equation (2.1) to (2.3), where the only space variable is the cylinder radius ρ and $x = \rho/a$ is the normalized radial variable : [7] :

$$\frac{3}{2}\frac{\partial(n_e T_e)}{\partial t} = \frac{1}{a^2}\frac{1}{x}\frac{\partial}{\partial x}(x n_e \chi_e \frac{\partial T_e}{\partial x}) - P_{sinks} + P_{sources}, \tag{2.1}$$

with boundary conditions,

$$\begin{aligned} \frac{\partial T_e}{\partial x}(0,t) &= 0, \forall t \geq 0 \\ T_e(1,t) &= T_{e,edge}(t), \forall t \geq 0 \end{aligned} \tag{2.2}$$

and the initial condition:

$$T_e(x,0) = T_0(x), \forall x \in [0,1] \tag{2.3}$$

Variable	*Description*	*Unit*
a	small plasma radius	m
B_ψ	poloidal magnetic field	T
B_ϕ	toroidal magnetic field	T
B_{ϕ_0}	toroidal magnetic field at the center	T
I_p	total plasma current	A
n_e	electron density profile	m^{-3}
n_i	ion density profile	m^{-3}
p_e	electron pressure profile	eVm^{-3}
P_{OH}	ohmic power density	W/m^3
P_{aux}	auxiliary sources power density	W/m^3
T_i	ions temperature profile	eV
T_e	electrons temperature profile	eV
x	normalized spatial variable	
e	electron charge, 1.6022×10^{-19}	C
m_e	electron mass, 9.1096×10^{-31}	kg
Ψ	poloidal magnetic flux	$T/m2$
Φ	toroidal magnetic flux	$T/m2$
q	safety factor	
s	magnetic shear	
V'	$V' \coloneqq \frac{\partial V}{\partial \rho}$, and V is the volume of a ρ surface	m^2
ι	inverse of the safety factor	
χ_e	electron diffusivity	m^2/s
ρ	spatial variable along the small plasma radius	m
ρ^*	The electron gyroradius	m
τ_E	global energy confinement time	s

Table 2.1: Relevant physical variables definition

$\chi_e(x,t)$ is the electron heat diffusivity, $P_{sources} = P_{OH} + P_{aux}$ is the supplied heating power density, P_{OH} is the ohmic effect power density, and P_{aux} is the auxiliary heating sources. P_{sinks} represents the lost power density such as electron-ion equipartition losses P_{ei} and radiation losses, and are be to be neglected since their dependence on the ion temperature evolution, this choice was made in [9] where other kinetic profiles T_i, n_e and n_i are kept fixed.

Because of the complexity of the heat transport dynamics, there is no fully analytic model for the heat diffusivity model. Instead, semi-empirical models have been proposed and tested on experimental data. For the control purposes we chose to use the bohm/gyrobohm model in [8] for χ_e :

$$\chi_e = \chi_{Be} + \chi_{gBe}, \tag{2.4}$$

where,

$$\chi_{Be} = \alpha_B \frac{T_e}{eB_{\phi_0}} {L^*_{p_e}}^{-1} \langle L^*_{T_e} \rangle^{-1} q^2, \quad {L^*_{p_e}}^{-1} = \frac{a|\nabla p_e|}{p_e}, \quad \langle L^*_{T_e} \rangle^{-1} = \frac{T_e(x=0.8) - T_e(x=1)}{T_e(x=1)}$$

$$\chi_{gBe} = \alpha_{gB} \frac{T_e}{eB_{\phi_0}} {L^*_{T_e}}^{-1} \rho^*, \quad \rho^* = \frac{m_e^{1/2} T_e^{1/2}}{eB_{\phi_0}}, \quad {L^*_{T_e}}^{-1} = \frac{a|\nabla T_e|}{T_e}$$

$p_e = n_e T_e$ being the electron pressure, χ_{gBe} the gyro-Bohm-like diffusivity, and χ_{Be} the diffusivity of the Bohm-like model multiplied by $\langle L^*_{T_e} \rangle^{-1}$, a parameter that tackle the non-local dependence by representing the phenomena in which the diffusivity increases when the edge temperature is decreased, and vice versa.

In order to decouple the $q(x,t)$ profile dynamics from the electron temperature profile in χ_{Be}, we choose q to be constant in time because of the slow and small time variations of the q profile compared to the T_e profile. We also consider a constant n_e profile as in [9] to deal only with T_e dynamics.

2.2 Edge transport model

In order to represent the *pedestal* behaviour corresponding to the H-mode, we extend the Bohm/gyro-Bohm model by introducing the effects of flow shearing rate together with the reduction of turbulence growth rate, and the magnetic shear s [20], that is to extend the model by adding a suppression function for the electron thermal difussivity (2.4) :

$$\chi_{e_s} = \chi_e \times f_s \tag{2.5}$$

The suppression function f_s is composed of two terms:

$$f_s = \frac{1}{1 + C\left(\frac{\omega_{E\times B}}{\gamma_{ITG}}\right)^2} \times \frac{1}{max(1, (s - s_{thres})^2)} \tag{2.6}$$

The first term represents the flow shearing rate through $\omega_{E\times B}$ and the reduction of the turbulence growth rate through the growth rate of ion temperature gradient γ_{ITG} [23]. The second term reduces the transport only in the region where the magnetic shear exceeds a specified threshold s_{thres}. To simplify the incorporation of this modification to the diffusivity model, the suppression function f_s was taken based on experimental results obtained in [20], and a 3rd order polynomial approximation is shown in Figure 2.1 :

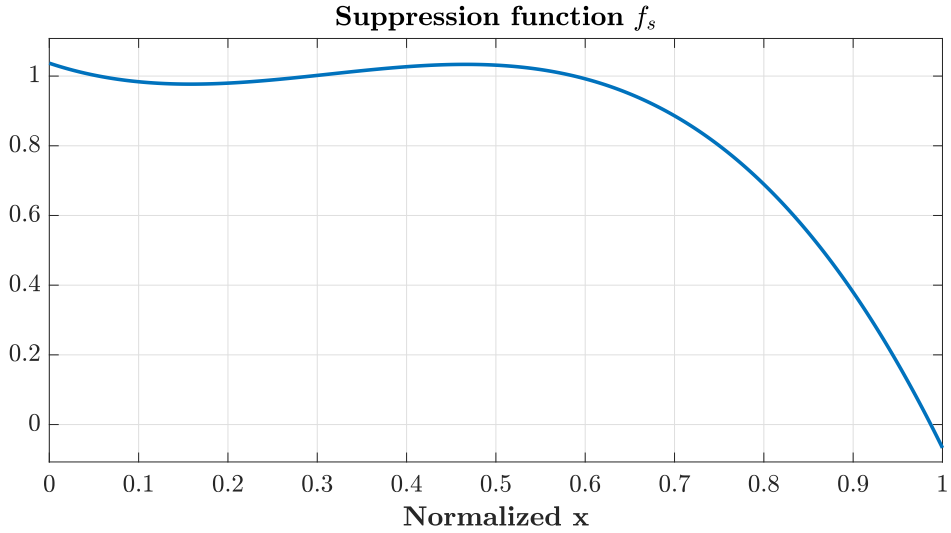

Figure 2.1: Polynomial approximation of the suppression function f_s in [20].

2.3 Model inputs

In the beginning of the discharge, the plasma heating comes from the induced plasma current I_p whose time evolution is computed offline and defines the discharge phases (ramp-up, flat-top and rump-down). The plasma current is not thus considered as an input to the system. On the other hand, the auxiliary heating sources such as EC and NBI are used for the online distributed control. They are subject to a profile shape constraint, and their power densities are approximated by weighted Gaussian distributions, for the case of ECH/ECCD antennas, we have for the $i-th$ actuator [9]:

$$P_{aux,i}(x,t) = P_i(t) \exp\left\{\frac{-4(x-x_{dep,i})^2}{w_{dep,i}^2}\right\} / \int_0^a \exp\left\{\frac{-4(x-x_{dep,i})^2}{w_{dep,i}^2}\right\} V' dx \quad (2.7)$$

with w_{dep} is the disposition width and ρ_{dep} is the location of the peak of the disposition. In most cases the x_{dep} and w_{dep} are fixed, and the amplitude of the power density for the i-th actuator $P_i(t)$ in (2.7) is used as an input in the model and:

$$P_{aux}(x,t) = \sum_i P_{aux,i}(x,t) \quad (2.8)$$

2.4 The control objectives

The objectives of this work are to :

- Analyze the stability of the nonlinear dynamics of the electron temperature model, using Lyapunov direct method and the sum of squares framework.
- Define the tracking problem of the electron temperature profile and guarantee asymptotic stability with a PI control input $u(x, t)$.
- Evaluate the controller in the RAPTOR simulator using constrained actuation, also with changing the reference profile, introducing disturbances and adding time delays to the system.

Chapter 3

Stability analysis and distributed control of the electron temperature profile

In this chapter, we use the direct Lyapunov stability method in an infinite-dimensional setting to analyze the stability of the nonlinear diffusion PDE presented in chapter 2, the resulting integral inequalities being verified using the sum of squares framework. Then we apply a distributed proportional-integral state feedback to a formulated tracking problem without taking into account the actuator constraints.

3.1 Stability analysis

In this section we present the formulation of the direct Lyapunov method for PDEs, as formulated in [12].

Definition 3.1.1. A dynamical system (nonlinear semi-group) on a compact normed space C is a family of maps $\{S(t)|C \to C, t \geq t_0\}$ such that :

- for each $t \geq t_0$, $S(t)$ is continuous from C to C,
- for each $u \in C$, the mapping $t \to S(t)u$ is continuous,
- $S(0)$ is the identity on C,
- $S(t)(S(\tau)u) = S(t+\tau)u$ for all $u \in C$ and all $t, \tau \geq 0$.

Definition 3.1.2. Let $\{S(t), t \geq t_0\}$ be a nonlinear semigroup on C and for any $u \in C$, let $Y(u) = \{S(t)u, t \geq t_0\}$ be the orbit through u. We say that u is an equilibrium point if $Y(u) = \{u\}$.

An orbit $Y(u)$ is stable if for any $\epsilon > 0$, there exists $\delta(\epsilon) > 0$ such that for all $t \geq t_0$, $||S(t)u - S(t)v||_C < \epsilon$ whenever $||u - v||_C < \delta(\epsilon)$, $v \in C$, where $||.||_C$ is the norm defined on C. An orbit is uniformly asymptotically stable if it is stable and also there is a neighbourhood $D = \{v \in C | ||u - v||_C < r\}$ such that $||S(t)u - S(t)v||_C \to 0$ as $t \to \infty$, uniformly for $v \in D$[1]. Similarly, it is exponentially stable if there exist $\beta,\ \gamma > 0$ such that :

$$||S(t)u - S(t)v||_C \leq \gamma ||u - v||_C e^{-\beta(t-t_0)},$$

for all $t \geq t_0$ and all $u,\ v \in C$.

Definition 3.1.3. Let $\{S(t), t \geq t_0\}$ be a nonlinear semigroup on C. A Lyapunov function is a continuous real-valued function V on C such that :

$$\dot{V}(u) = \lim_{t \to 0^+} \frac{V(S(t)u) - V(u)}{t} \leq 0,$$

for all $u \in C$.

Now considering the fallowing PDE :

$$\frac{\partial u}{\partial t} = \mathcal{A}u, \qquad u(t_0, x) = u_0(t) \in \mathcal{M} \subset \mathcal{H}^q([0, 1]) \tag{3.1}$$

Where $\mathcal{A}$ is a nonlinear operator defined in $\mathcal{M}$.

Theorem 1. Suppose there is a function $V(u) \in \mathcal{C}^1$, with $V(0) = 0$, and scalars $c_1,\ c_2,\ c_3 \in \mathbb{R}_{>0}$ such that :

$$c_1 ||u||_q^2 \leq V(u) \leq c_2 ||u||_q^2 \tag{3.2}$$

$$\dot{V}(u) < 0 \tag{3.3}$$

then, (3.1) is asymptotically stable, and if we have also

$$\dot{V}(u) < -c_3 ||u||_q^2 \tag{3.4}$$

then, (3.1) is exponentially stable, and we have :

$$||u(t, x)||_q^2 \leq \frac{c_2}{c_1} ||u_0(x)||_q^2 e^{-\frac{c_3}{c_1}(t-t_0)} \tag{3.5}$$

3.2 Integral inequalities of polynomial integrands

(The notations for this section are listed in Appendix A, and the section formulation is detailed in [24])

Consider the nonlinear operator $\mathcal{A}$ in (3.1) to be polynomial in the dependent variable u , i.e :

$$\frac{\partial u}{\partial t} = F(x, D^\alpha u), \qquad u(t_0, x) = u_0(x) \in \mathcal{M} \subset \mathcal{H}^2([0,1]) \tag{3.6}$$

where $F(x, D^\alpha u)$ is polynomial on $D^\alpha u$. Consider a P-weighted candidate Lyapunov function of the form :

$$V(u) = \frac{1}{2}||u||^2_{q,P(x)} = \frac{1}{2}\int_0^1 (D^q u)^T P(x)(D^q u)\ dx, \qquad P(x) > 0 \quad \forall x \in [0,1] \tag{3.7}$$

then we have (3.2) satisfied with $c_1 = min_{[0,1]}(\lambda_{min}(P(x))$, and $c_2 = max_{[0,1]}(\lambda_{max}(P(x))$, and to prove asymptotic stability, one should verify that :

$$-\int_0^1 (D^q u)^T P(x) F(x, D^\alpha u) + F(x, D^\alpha u) P(x)(D^q u)\ dx > 0 \tag{3.8}$$

In more compact and general form, we want to verify that :

$$\int_0^1 f(x, D^\alpha u(x))\ dx \geq 0 \tag{3.9}$$

where $f(., z) \in \mathcal{R}[z]$, and $u(x) \in \mathcal{M}(Q)$, a subset of $\mathcal{H}^q$ satisfying the boundary conditions :

$$Q \begin{pmatrix} D^{\alpha-1}u(1) \\ D^{\alpha-1}u(0) \end{pmatrix} = 0 \tag{3.10}$$

Writing f in (3.9) in quadratic-like form and adding terms due to the non-uniqueness of the integral expression, we rewrite (3.9) as:

$$\int_0^1 \left[\left(\xi^{\lceil \frac{k}{2} \rceil}(D^\alpha u(x))\right)^T F(x)\ \xi^{\lceil \frac{k}{2} \rceil}(D^\alpha u(x)) + \frac{d}{dx}\left(\left(\xi^{\lceil \frac{k}{2} \rceil}(D^{\alpha-1} u(x))\right)^T H(x)\ \xi^{\lceil \frac{k}{2} \rceil}(D^{\alpha-1} u(x)) \right) \right] dx$$
$$+ \left[\left(\xi^{\lceil \frac{k}{2} \rceil}(D^{\alpha-1} u(x))\right)^T H(x)\ \xi^{\lceil \frac{k}{2} \rceil}(D^{\alpha-1} u(x)) \right]_1^0 \geq 0 \tag{3.11}$$

where $k = deg(f(.,z))$, $n = \dim(u)$, $F\colon [0,1] \to \mathbb{S}^{\sigma(n\alpha,\lceil \frac{k}{2} \rceil)}$, $H\colon [0,1] \to \mathbb{S}^{\sigma(n(\alpha-1),\lceil \frac{k}{2} \rceil)}$. After manipulation of (3.2), we have :

$$\begin{aligned}&\int_0^1 \left(\xi^{\lceil \frac{k}{2} \rceil}(D^\alpha u(x))\right)^T (F(x) + \bar{H}(x))\ \xi^{\lceil \frac{k}{2} \rceil}(D^\alpha u(x))\ dx \\ &+ \begin{bmatrix}\xi^{\lceil \frac{k}{2} \rceil}(D^{\alpha-1}u(0))\\ \xi^{\lceil \frac{k}{2} \rceil}(D^{\alpha-1}u(1))\end{bmatrix}^T \begin{bmatrix}H(0) & 0\\ 0 & -H(1)\end{bmatrix} \begin{bmatrix}\xi^{\lceil \frac{k}{2} \rceil}(D^{\alpha-1}u(0))\\ \xi^{\lceil \frac{k}{2} \rceil}(D^{\alpha-1}u(1))\end{bmatrix} \geq 0 \end{aligned} \tag{3.12}$$

with :

$$\bar{H}(x) = M_T^T \left(\frac{d}{dx}H(x)\right) M_T + M_T^T H(x) M_{Td} + M_{Td}^T H(x) M_T, \tag{3.13}$$

$$M_T \xi^{\lceil \frac{k}{2} \rceil}(D^\alpha u(x)) = \xi^{\lceil \frac{k}{2} \rceil}(D^{\alpha-1}u(x)), \quad M_{Td}\xi^{\lceil \frac{k}{2} \rceil}(D^\alpha u(x)) = \frac{d}{dx}\xi^{\lceil \frac{k}{2} \rceil}(D^{\alpha-1}u(x)) \tag{3.14}$$

Therefore, if we can find $P(x) > 0,\ \forall x \in [0,1]$, and $H(x) \in \mathcal{C}^1([0,1])$ such that:

$$F(x) + \bar{H}(x) \geq 0, \quad \forall x \in [0,1], \tag{3.15}$$

and

$$\begin{bmatrix}\xi^{\lceil \frac{k}{2} \rceil}(D^{\alpha-1}u(0))\\ \xi^{\lceil \frac{k}{2} \rceil}(D^{\alpha-1}u(1))\end{bmatrix}^T \begin{bmatrix}H(0) & 0\\ 0 & -H(1)\end{bmatrix} \begin{bmatrix}\xi^{\lceil \frac{k}{2} \rceil}(D^{\alpha-1}u(0))\\ \xi^{\lceil \frac{k}{2} \rceil}(D^{\alpha-1}u(1))\end{bmatrix} \geq 0 \tag{3.16}$$

then (3.9) holds $\forall u \in \mathcal{M}(Q)$.

Now, to verify (3.15), we assume that $F(x)$ has a polynomial dependence on x, and we impose that also to $H(x)$ so we can use Positivstellensatz [22] to test for (3.15) on $\{x|w(x) := x(x-1) \geq 0\}$ $(x \in [0,1])$ in terms of SOS polynomial matrices, that is to verify :
if there exists $N(x) \in \Sigma^{n_F \times n_F}[x]$ $(n_F = \sigma(n\alpha, \lceil \frac{k}{2} \rceil))$ such that:

$$F(x) + \bar{H}(x) - N(x)w(x) \in \Sigma^{n_F \times n_F}[x] \tag{3.17}$$

The feasibility problem of finding $P(x) > 0,\ \forall x \in [0,1]$, and $H(x) \in \mathcal{C}^1([0,1])$ and $N(x) \in \Sigma[x]$ with constraints (3.17) and (3.16) is then solved using SOSTOOLS [21] and INTSOSTOOLS plug-in [25].

3.3 Open loop stability of the electron temperature profile

In this section, we propose a Lyapunov function candidate and we test the resulting integral inequalities using the framework described in 3.2 to study the stability of the electron temperature profile in open loop.

We consider the Lyapunov function candidate :

$$V(T_e) = \frac{1}{2}||T_e||^2_{2,P(x)} = \frac{1}{2}\int_0^1 x^2 P(x) T_e^2 \, dx, \qquad P(x) > 0 \quad \forall x \in [0,1] \tag{3.18}$$

Where T_e represents the electron temperature and its dynamics is described by the PDE (with $u = 0$):

$$\frac{\partial T_e}{\partial t} = \frac{A}{x}\frac{\partial}{\partial x}\left(x\left(B(x)\frac{\partial T_e}{\partial x} + C(x)\sqrt{T_e}\frac{\partial T_e}{\partial x}\right)\frac{\partial T_e}{\partial x}\right), \quad \forall x \in [0,1] \tag{3.19}$$

with boundary conditions,

$$\begin{aligned} \frac{\partial T_e}{\partial x}(0,t) &= 0, \forall t \geq 0 \\ T_e(1,t) &= 0, \forall t \geq 0 \end{aligned} \tag{3.20}$$

where:

$$A = \frac{2}{3a^2 n_{e,av}}, \tag{3.21}$$

$$B(x) = q^2(x) f_s(x) \frac{a\alpha_B n_{e,av}}{eB_{\phi_0}} L_{T_e}, \tag{3.22}$$

$$C(x) = f_s(x) \frac{a\alpha_{gB} m_e^{1/2} n_{e,av}}{(eB_{\phi_0})^2} \tag{3.23}$$

$n_{e,av}$ is taken as the average over x of the constant $n_e(x)$ profile to impose polynomial dependency of the expression in x. Similarly, $q(x)$ is a polynomial approximation of the time-average of a RAPTOR simulation $q(x,t)$ profile, and L_{T_e} is a time average for $\langle L^*_{T_e} \rangle^{-1}$ in (2.4).
Then we have:

$$\dot{V}(T_e) = \int_0^1 x^2 P(x) \frac{\partial T_e}{\partial x} T_e \, dx, \qquad P(x) > 0 \quad \forall x \in [0,1] \tag{3.24}$$

In order to use the sum of squares framework to find $P(x)$ that makes $\dot{V}(T_e) < 0$, we need to do a final modification to the PDE to impose polynomial dependence of the integrand of $\dot{V}(T_e)$ in $D^q(T_e)$ ($\sqrt{T_e} \to T_e$), so we prove the stability of:

$$\frac{\partial \mathcal{T}_e}{\partial t} = \frac{A}{x}\frac{\partial}{\partial x}\left(x\left(B(x)\frac{\partial \mathcal{T}_e}{\partial x} + C(x)\underline{\mathcal{T}_e}\frac{\partial \mathcal{T}_e}{\partial x}\right)\frac{\partial \mathcal{T}_e}{\partial x}\right), \quad \forall x \in [0,1] \tag{3.25}$$

then we make sure that :

$$\dot{V}(T_e) = \dot{V}(\mathcal{T}_e) + \int_0^1 x^2 P(x) T_e \left(\frac{\partial T_e}{\partial x} - \frac{\partial \mathcal{T}_e}{\partial x}\right) dx < 0 \tag{3.26}$$

by verifying that:

$$\int_0^1 x^2 P(x) T_e \left(\frac{\partial T_e}{\partial x} - \frac{\partial \mathcal{T}_e}{\partial x}\right) dx \leq 0 \tag{3.27}$$

Now that all is setup, we start by rewriting the integrand of :

$$\dot{V}(\mathcal{T}_e) = \int_0^1 x^2 P(x) \frac{\partial \mathcal{T}_e}{\partial x} \mathcal{T}_e \, dx \tag{3.28}$$

in a quadratic-like form. After integration by parts we have:

$$\dot{V}(\mathcal{T}_e) = \int_0^1 \begin{bmatrix} \mathcal{T}_e \\ \frac{\partial \mathcal{T}_e}{\partial x} \\ \mathcal{T}_e \frac{\partial \mathcal{T}_e}{\partial x} \\ (\frac{\partial \mathcal{T}_e}{\partial x})^2 \end{bmatrix}^T \begin{bmatrix} 0 & 0 & 0 & \frac{\alpha_4}{4} \\ 0 & 0 & \frac{\alpha_4}{4} & \frac{\alpha_1}{2} \\ 0 & \frac{\alpha_4}{4} & \alpha_3 & \frac{\alpha_2}{2} \\ \frac{\alpha_4}{4} & \frac{\alpha_1}{2} & \frac{\alpha_2}{2} & 0 \end{bmatrix} \begin{bmatrix} \mathcal{T}_e \\ \frac{\partial \mathcal{T}_e}{\partial x} \\ \mathcal{T}_e \frac{\partial \mathcal{T}_e}{\partial x} \\ (\frac{\partial \mathcal{T}_e}{\partial x})^2 \end{bmatrix} dx \tag{3.29}$$

With :

$$\alpha_1 = -x^2 B(x) P(x) A, \tag{3.30}$$

$$\alpha_2 = -x^2 C(x) P(x) A, \tag{3.31}$$

$$\alpha_3 = -x C(x) P(x) A - x^2 C(x) P'(x) A, \tag{3.32}$$

$$\alpha_4 = -x B(x) P(x) A - x^2 B(x) P'(x) A \tag{3.33}$$

Using SOSTOOLS and INTSOSTOOLS, we compute the polynomial $P(x)$ shown in Figure 3.1 that makes $\dot{V}(\mathcal{T}_e) < 0$. After that we verify (3.27) by simulation for various relevant initial conditions, which is not a proof but should be sufficient in our case.

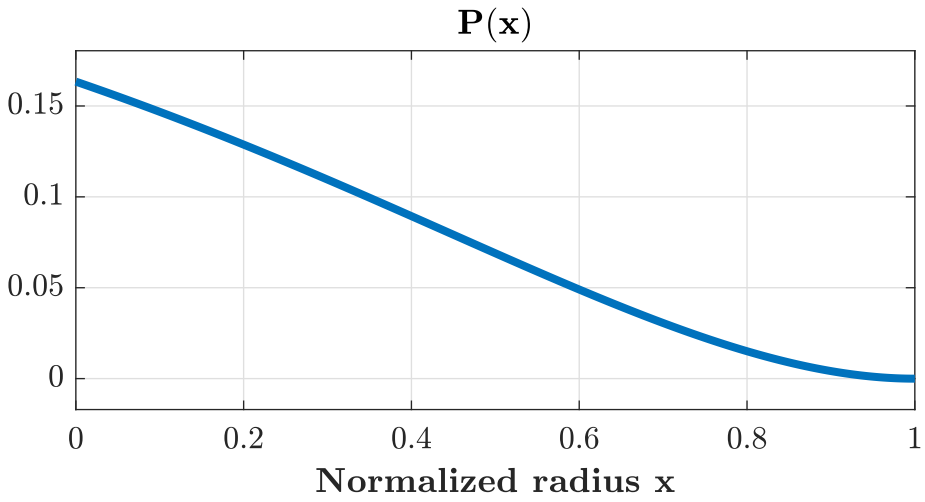

Figure 3.1: Numerical solution of $P(x)$.

3.4 Distributed control and closed loop stability

Now that we discussed the stability of the open loop system, we will study the stability of the system when we close the loop with a PI controller. First we formulate the tracking problem, then we study the stability of the closed loop system.

Let $\mathcal{D}(t, x, \mathcal{T}_e)$ be the dynamics of $\mathcal{T}_e$ and u the input, then:

$$\frac{\partial \mathcal{T}_e}{\partial t} = \mathcal{D}(t, x, \mathcal{T}_e) + u \tag{3.34}$$

and given a reference temperature profile $r(x)$, the error model can be written as:

$$\mathcal{E}(t, x) = \mathcal{T}_e - r(x) \quad and \tag{3.35}$$

$$\frac{\partial \mathcal{E}}{\partial t} = \mathcal{D}(t, x, \mathcal{E} + r) + u \tag{3.36}$$

Given the polynomial dependence of $\mathcal{D}(t, x, u)$ in $D^q u$, we have that :

$$\frac{\partial \mathcal{E}}{\partial t} = \mathcal{D}(t, x, \mathcal{E}) + \mathcal{R}_{est}(t, x, \mathcal{E}, r) + u \tag{3.37}$$

where:

$$\mathcal{R}_{est}(t,x,\mathcal{E},r) =$$
$$\frac{A}{x}\frac{\partial}{\partial x}\left(xB(x)\left(\left(\frac{\partial r}{\partial x}\right)^2+2\frac{\partial \mathcal{E}}{\partial x}\frac{\partial r}{\partial x}\right)+xC(x)(\mathcal{E}+r)\left(\left(\frac{\partial \mathcal{E}}{\partial x}\right)^2+\left(\frac{\partial r}{\partial x}\right)^2+2\frac{\partial \mathcal{E}}{\partial x}\frac{\partial r}{\partial x}\right)-xC(x)\mathcal{E}\left(\frac{\partial \mathcal{E}}{\partial x}\right)^2\right) \tag{3.38}$$

and we define the feedback control input as :

$$u_{des} = -\mathcal{R}_{est}(t,x,\mathcal{E},r) - \alpha_P\mathcal{E} - \int_{t_0}^{t}\alpha_I\mathcal{E}dt \tag{3.39}$$

The resulting system is then

$$\begin{cases} \frac{\partial \mathcal{E}}{\partial t} &= \mathcal{D}(t,x,\mathcal{E}) - \alpha_P\mathcal{E} + I \\ \frac{\partial I}{\partial t} &= -\alpha_I\mathcal{E} \end{cases} \tag{3.40}$$

and we consider the Lyapunov candidate :

$$V(\mathcal{T}_e, I) = \frac{1}{2}\int_0^1 x^2 P_T(x)\mathcal{T}_e^2\ dx + \frac{1}{2}\int_0^1 x^2 P_I(x) I^2\ dx, \tag{3.41}$$
$$P_T(x) > 0 \ and \ P_I(x) > 0 \quad \forall x \in [0,1]$$

and we formulate $\dot{V}(\mathcal{T}_e, I)$ in quadratic-like form:

$$\dot{V}(\mathcal{T}_e, I) = \int_0^1 \begin{bmatrix} \mathcal{T}_e \\ \frac{\partial \mathcal{T}_e}{\partial x} \\ \mathcal{T}_e\frac{\partial \mathcal{T}_e}{\partial x} \\ (\frac{\partial \mathcal{T}_e}{\partial x})^2 \\ I \end{bmatrix}^T \begin{bmatrix} \alpha_5 & 0 & 0 & \frac{\alpha_4}{4} & \frac{\alpha_6}{2} \\ 0 & 0 & \frac{\alpha_4}{4} & \frac{\alpha_1}{2} & 0 \\ 0 & \frac{\alpha_4}{4} & \alpha_3 & \frac{\alpha_2}{2} & 0 \\ \frac{\alpha_4}{4} & \frac{\alpha_1}{2} & \frac{\alpha_2}{2} & 0 & 0 \\ \frac{\alpha_6}{2} & 0 & 0 & 0 & 0 \end{bmatrix} \begin{bmatrix} \mathcal{T}_e \\ \frac{\partial \mathcal{T}_e}{\partial x} \\ \mathcal{T}_e\frac{\partial \mathcal{T}_e}{\partial x} \\ (\frac{\partial \mathcal{T}_e}{\partial x})^2 \\ I \end{bmatrix} dx \tag{3.42}$$

given :

$$\alpha_5 = -x^2 P_T(x)\alpha_P, \tag{3.43}$$
$$\alpha_6 = x^2\left(P_T(x) - \alpha_I P_I(x)\right), \tag{3.44}$$

and the other α's are the same with $P_T(x)$ instead of $P(x)$.

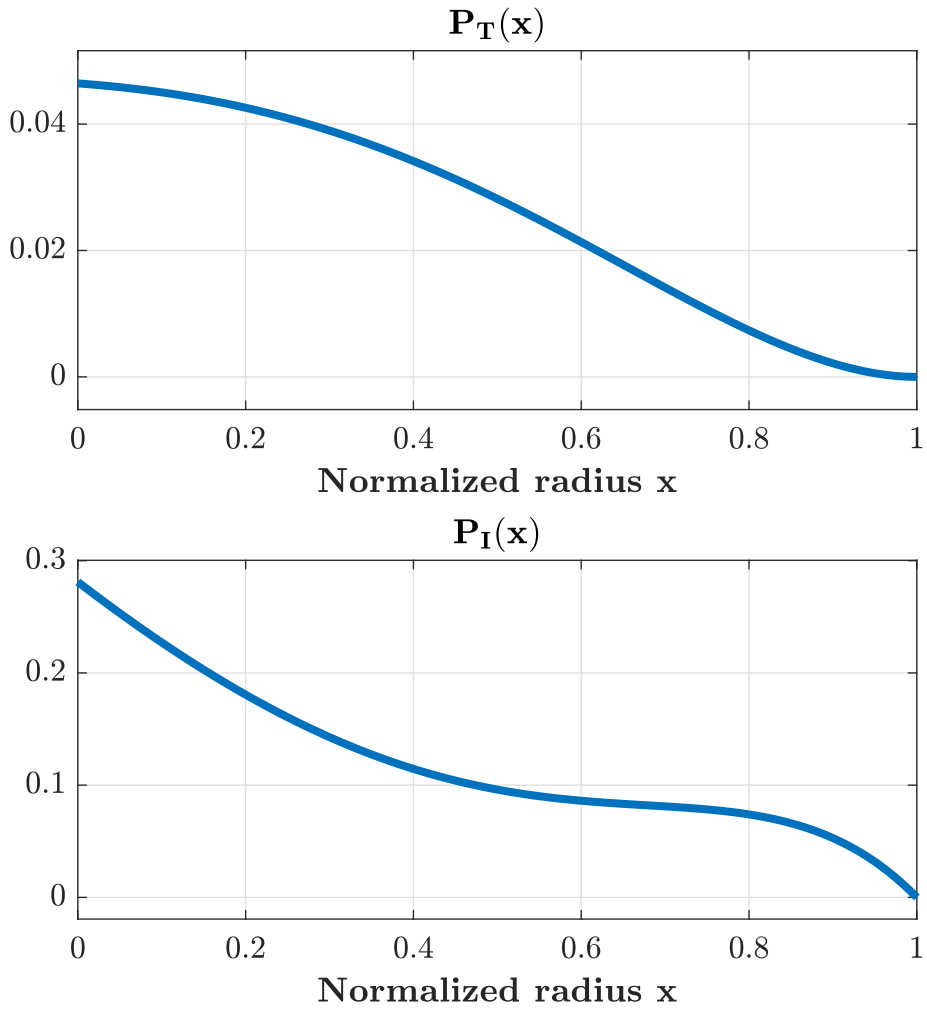

Figure 3.2: Numerical solutions of $P_T(x)$ and $P_I(x)$

Since we are formulating the problem as a feasibility problem and not as an optimization one, we use some given P and I parameters that are tested on RAPTOR and give good performances. The stability of the closed loop system is then verified, and the resulting $P_T(x)$ and $P_I(x)$ are shown in Figure 3.2.

Chapter 4

Control implementation and results

After discussing the stability of the closed loop system in the previous chapter, we aim in this chapter to implement the control strategy on the RAPTOR simulator with TCV tokamak settings. RAPTOR is a lightweight code that is used to simulate simplified nonlinear plasma transport physics, and is also used as a real-time state observer for the TCV tokamak. We first introduce the RAPTOR configuration used for the simulation, then we formulate an optimization problem to find the engineering parameters to apply as inputs to the system, and finally we present the results of the simulation where we test the performance and robustness of the controller by adding disturbances and time delays.

4.1 RAPTOR configuration

We use a configuration where the plasma current rumps up from 80 kA to 120 kA and we use two EC antennas as auxiliary sources, with power amplitude $P_1(t)$ and $P_2(t)$, the first one is a pure ECH heating source located at $x_{dep} = 0$ with deposition angle of $w_{dep} = 0.35$, and the second one is an ECCD current drive source with $x_{dep} = 0.4$ and $w_{dep} = 0.35$. The engineering inputs $P_1(t)$ and $P_2(t)$ are limited to 1 MW.

For the heat diffusivity χ_e we choose the model introduced in [14] (equation 13 in the paper), with H-mode parameters that are used in the paper to fit a H-mode T_e profile in TCV tokamak. In Figure 4.1 we see the difference in the T_e profile between an L-mode simulation using the RAPTOR standard transport model, and the pedestal at the edge in the H-mode simulation.

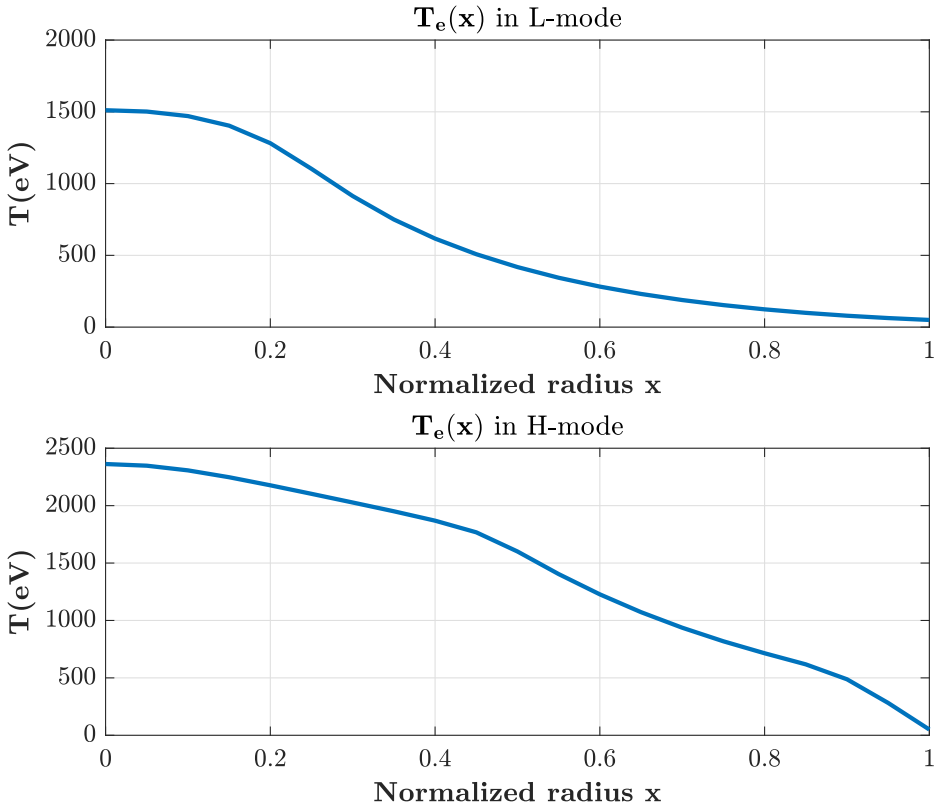

Figure 4.1: L-mode and H-mode simulation of $T_e(x)$ in RAPTOR

4.2 Control implementation

The H-mode profile in 4.1 is obtained when applying $P_1 = 100$ kW and $P_2 = 100$ kW, where the radial distributions of these ECH/ECCD auxiliary sources are shown in Figure 4.2. Since the actual system input is $u_{ac} = [P_1, P_2]^T$, we need to find these

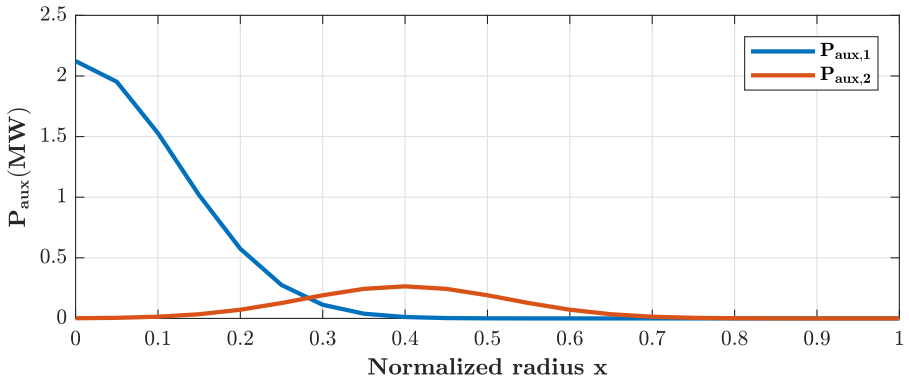

Figure 4.2: Auxiliary ECH/ECCD sources distributions.

amplitudes that minimize the error between the desired control input u_{des} calculated

in (3.39) and the achievable input P_{aux} in (2.7) and (2.8). This is done by solving the following optimization problem:

$$u_{ac}^{*} = arg\min_{u_{ac}} \int_{0}^{1} \left(u_{des} - P_{aux}(u_{ac})\right)^2 dx \tag{4.1}$$

subject to :

$$0 \leq P_1 \leq 1\text{MW}$$
$$0 \leq P_2 \leq 1\text{MW}$$

and we solve this problem with the MATLAB optimization routine `fmincon`.

4.3 Simulation results

In this section we present the simulation results with different scenarios in order to test the performance and the robustness of the control algorithm while we compare the open loop and the closed loop responses. The controller parameters used in all simulations are $\alpha_P = 2 \times 10^5$ and $\alpha_I = 4 \times 10^3$.

In Figure 4.3, we see the time evolution of the T_e profile in various space points and the final profile, as well as the time evolution of u_{ac} that solves the optimization problem (4.1). We see that the tracking performance in closed-loop is improved compared to the open loop case. The time response in closed loop is further reduced in the region where the actuators are disposed ($x_{dep} = 0$ and $x_{dep} = 0.4$). From the time evolution of u_{ac}, we see that the optimization routine retrieved the original values $P_1 = 0.1$ MW and $P_2 = 0.1$ MW with a short saturation.

4.3.1 Changing the reference profile and adding disturbance

To test the behaviour of the controller when changing the operational point we used a 2 stages reference profile. The controller disturbance attenuation is tested by adding a third ECCD source at $x_{dep} = 0.2$ with $w_{dep} = 0.35$ and $P_3 = 0.1$ MW at $t = 0.4$ s. The results are shown in Figure 4.4, where we see the effect of the integral control in reducing the steady-state error.

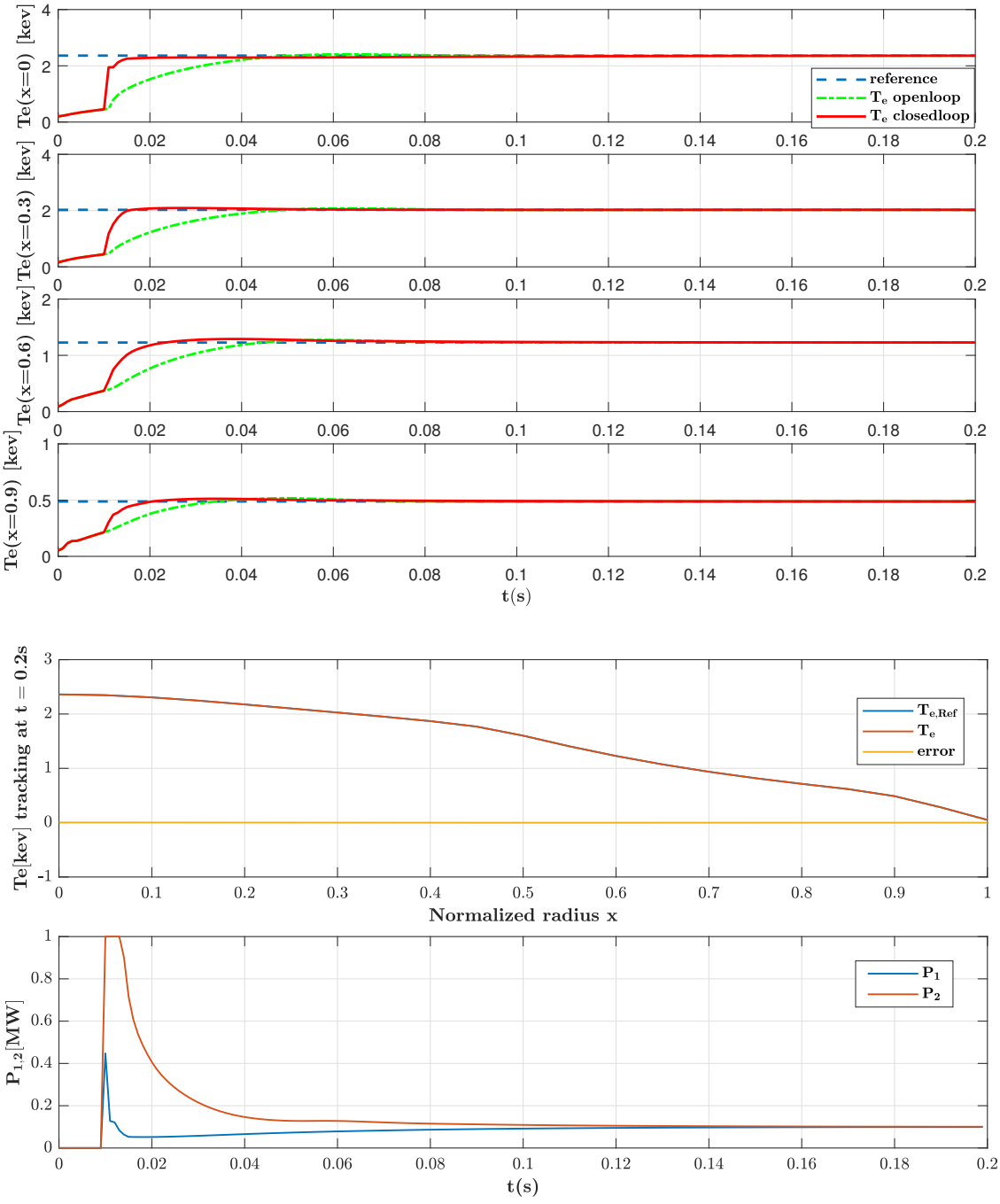

Figure 4.3: T_e tracking and $P_{1,2}$ time evolution.

4.3.2 Adding time delays

Because of the fast dynamics of the system, the transportation of the control signal might be considered as a time delay, for that we consider a delay of 3 ms in the control loop, and in Figure 4.5 we see the deterioration of the performance in presence of such

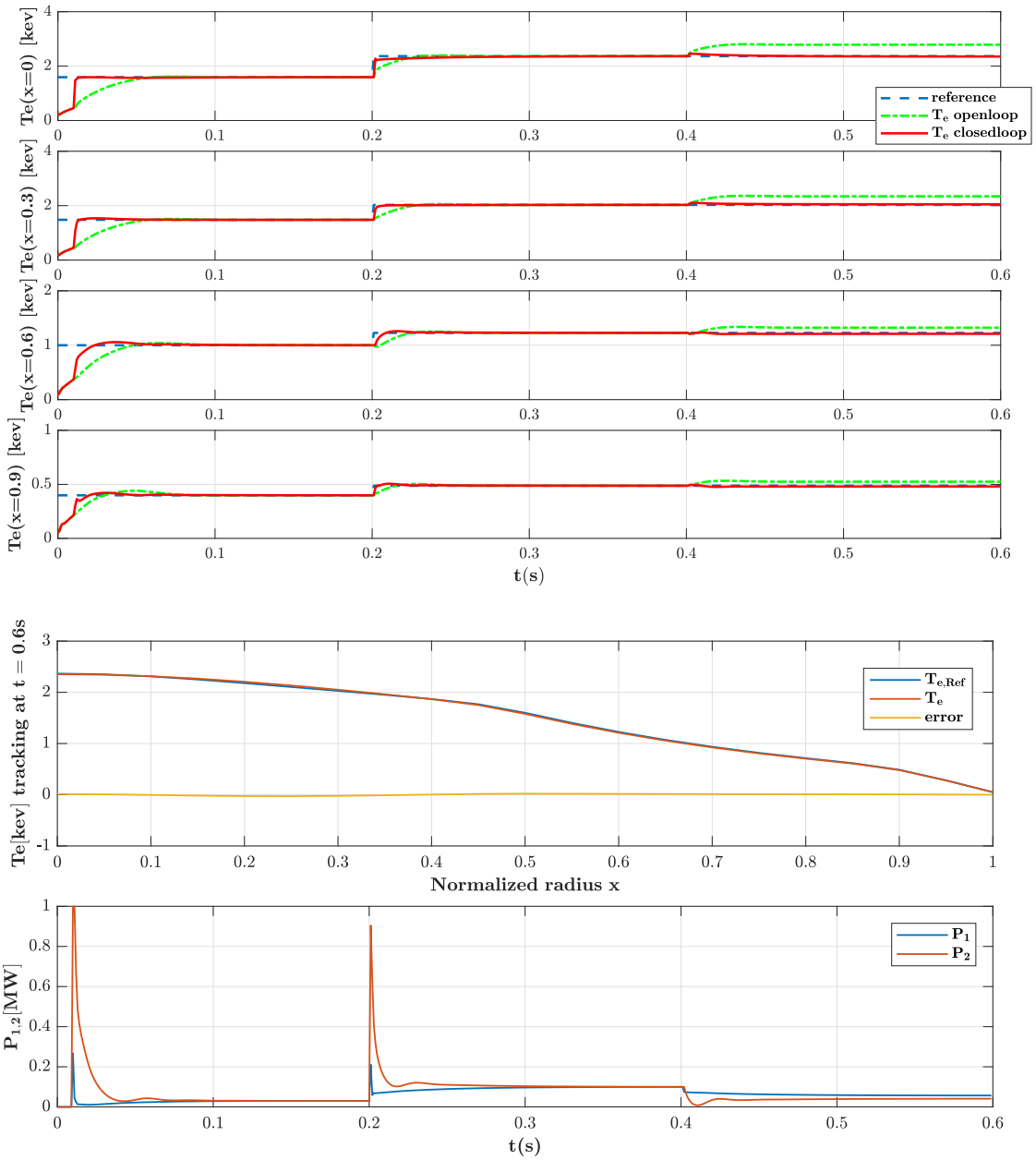

Figure 4.4: T_e tracking and $P_{1,2}$ time evolution when changing set point and introducing disturbance at $t = 0.4$ s.

delay that in this case represents more than a tenth of the response time in closed-loop.

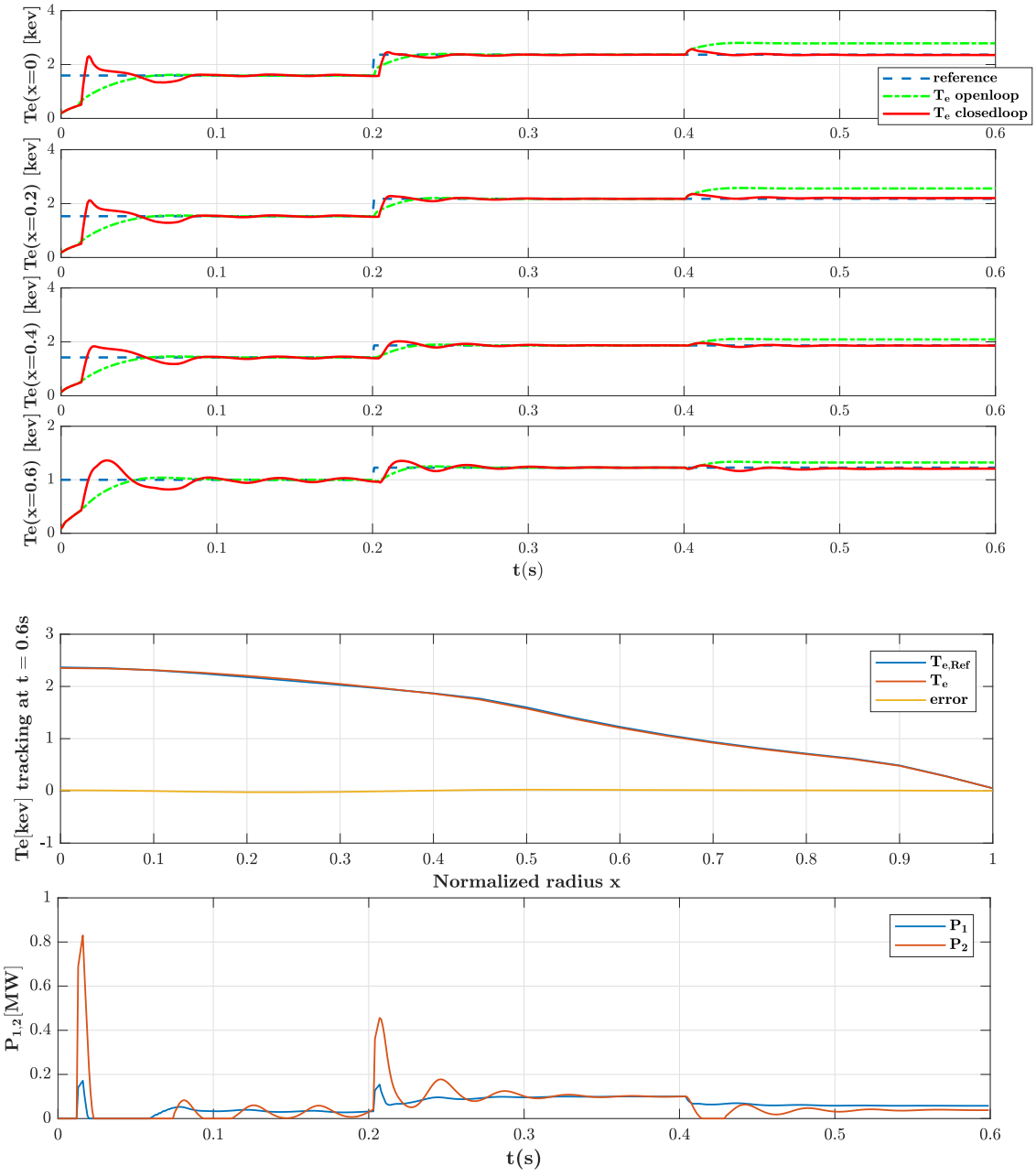

Figure 4.5: T_e tracking and $P_{1,2}$ time evolution when changing set point and introducing disturbance at $t = 0.4$ s and time delays of 3 ms.

Chapter 5

Conclusions and future work

5.1 Conclusions

In this thesis, the stability analysis and control of the electron temperature profile in tokamak plasmas was addressed, where the dynamics is described by first-principle control-oriented model with a modification of the transport model to represent the H-mode pedestal.

The stability of the resulting nonlinear parabolic PDE was studied with a weighted Lyapunov function candidate. A sum of squares framework used to compute the weighting functions that ensure the positivity of the resulting integral inequalities.

As for the control part, a PI controller was used to ensure a good tracking of the electron temperature profile in closed loop. The stability of the closed loop system was also tackled. To evaluate the control strategy, RAPTOR plasma simulator was used and the control input constraints was taken into account to derive the engineering control parameters. The simulation results show good performance of the controller in tracking the H-mode TCV plasma electron temperature profile, also the robustness of the controller with respect to changing reference profile, disturbance presence and adding time delay has been tested.

5.2 Future work

Mainly in the infinite dimensional control approach, there are many challenges that need to be tackled, namely:

- Considering the coupling between the plasma profiles as well as the two time-scales dynamics.

- Investigating transport models that describe internal transport barrier (ITB) scenarios.
- The use of more elaborate control strategies, boundary control, and the consideration of experimental validation on tokamaks.

Appendix A

Notations for section 3.2

The ring of polynomials and the ring of sum of squares polynomials on a real variable x are denoted $\mathcal{R}[x]$ and $\Sigma[x]$, respectively.

The ring of SOS square matrices of dimention n, i.e, matrices $M(x) \in \mathcal{R}^{n\times n}[x]$, satisfying $M(x) = \sum_{i=1}^{n_M} N_i^T(x)N_i(x)$ with $N_i(x) \in \mathcal{R}^{d_i\times n}$, is denoted $\Sigma^{n\times n}[x]$.

For a vector containing all monomials in $w_n = (w_1, w_2, ..., w_n) \in \mathbb{R}^n$ up to degree k, $\xi^k(w)$, its cardinality is denoted $\sigma(n,k) \coloneqq \sum_{i=0}^{k} \binom{n+i-1}{n-1} = \sum_{i=0}^{k} \frac{(n+i-1)!}{(n-1)!i!}$.

For $u \in \mathcal{C}^\alpha(\Omega),\ \alpha \in \mathbb{N}_{>0}$, define $D^\alpha u \coloneqq (u, \partial_x u, ..., \partial_x^\alpha u)$.

The set of real symmetric matrices is denoted $\mathbb{S}^n \coloneqq \{A \in \mathbb{R}^{n\times n} | A = A^T\}$.

The ceil function is denoted $\lceil . \rceil$.

Bibliography

[1] Bp (2016). bp statistical review of world energy 2016. [online] london: Bp statistical review of world energy. Available at: `http://www.bp.com/statisticalreview`.

[2] Eia (2017). international energy outlook 2017. Available at: `https://www.eia.gov/outlooks/ieo/`.

[3] F. B. Argomedo, E. Witrant, C. Prieur, S. Brémond, R. Nouailletas, and J.-F. Artaud. Lyapunov-based distributed control of the safety-factor profile in a tokamak plasma. *Nuclear Fusion*, 53(3):033005, 2013.

[4] M. D. Boyer, J. Barton, E. Schuster, T. C. Luce, J. R. Ferron, M. L. Walker, D. A. Humphreys, B. G. Penaflor, and R. D. Johnson. First-principles-driven model-based current profile control for the diii-d tokamak via lqi optimal control. *Plasma Physics and Controlled Fusion*, 55(10):105007, 2013.

[5] P. D. Christofides. Control of nonlinear distributed process systems: Recent developments and challenges. *AIChE Journal*, 47(3):514–518, 2001.

[6] P. D. Christofides. *Nonlinear and robust control of PDE systems: Methods and applications to transport-reaction processes*. Springer Science & Business Media, 2012.

[7] A. Clémençon, C. Guivarch, S. Eury, X. Zou, and G. Giruzzi. Analytical solution of the diffusion equation in a cylindrical medium with step-like diffusivity. *Physics of plasmas*, 11(11):4998–5009, 2004.

[8] M. Erba, A. Cherubini, V. Parail, E. Springmann, and A. Taroni. Development of a non-local model for tokamak heat transport in l-mode, h-mode and transient regimes. *Plasma Physics and Controlled Fusion*, 39(2):261, 1997.

[9] F. Felici. Real-time control of tokamak plasmas: from control of physics to physics-based control. 2011.

[10] F. Felici, O. Sauter, S. Coda, B. Duval, T. Goodman, J. Moret, J. Paley, T. Team, et al. Real-time physics-model-based simulation of the current density profile in tokamak plasmas. *Nuclear Fusion*, 51(8):083052, 2011.

[11] O. Gaye, L. Autrique, Y. Orlov, E. Moulay, S. Brémond, and R. Nouailletas. H stabilization of the current profile in tokamak plasmas via an lmi approach. *Automatica*, 49(9):2795–2804, 2013.

[12] D. Henry. *Geometric theory of semilinear parabolic equations*, volume 840. Springer, 2006.

[13] M. Keilhacker. H-mode confinement in tokamaks. *Plasma Physics and Controlled Fusion*, 29(10A):1401, 1987.

[14] D. Kim, A. Merle, O. Sauter, and T. Goodman. Simple predictive electron transport models applied to sawtoothing plasmas. *Plasma Physics and Controlled Fusion*, 58(5):055002, 2016.

[15] B. Mavkov, E. Witrant, and C. Prieur. Distributed control of coupled inhomogeneous diffusion in tokamak plasmas (full version). 2017.

[16] D. Moreau, D. Mazon, M. Ariola, G. De Tommasi, L. Laborde, F. Piccolo, F. Sartori, T. Tala, L. Zabeo, A. Boboc, et al. A two-time-scale dynamic-model approach for magnetic and kinetic profile control in advanced tokamak scenarios on jet. *Nuclear Fusion*, 48(10):106001, 2008.

[17] D. Moreau, D. Mazon, M. Walker, J. Ferron, K. Burrell, S. Flanagan, P. Gohil, R. Groebner, A. Hyatt, R. La Haye, et al. Plasma models for real-time control of advanced tokamak scenarios. *Nuclear Fusion*, 51(6):063009, 2011.

[18] D. Moreau, M. L. Walker, J. R. Ferron, F. Liu, E. Schuster, J. E. Barton, M. D. Boyer, K. H. Burrell, S. Flanagan, P. Gohil, et al. Integrated magnetic and kinetic control of advanced tokamak plasmas on diii-d based on data-driven models. *Nuclear Fusion*, 53(6):063020, 2013.

[19] J. Ongena, R. Koch, R. Wolf, and H. Zohm. Magnetic-confinement fusion. *Nature Physics*, 12(5):398, 2016.

[20] Y. Pianroj and T. Onjun. Simulations of h-mode plasmas in tokamak using a complete core-edge modeling in the baldur code. *Plasma Science and Technology*, 14(9):778, 2012.

[21] S. Prajna, A. Papachristodoulou, and P. A. Parrilo. Introducing sostools: A general purpose sum of squares programming solver. In *Decision and Control, 2002, Proceedings of the 41st IEEE Conference on*, volume 1, pages 741–746. IEEE, 2002.

[22] M. Putinar. Positive polynomials on compact semi-algebraic sets. *Indiana University Mathematics Journal*, 42(3):969–984, 1993.

[23] M. Sugihara, Y. Igitkhanov, G. Janeschitz, G. Pacher, H. Pacher, G. Pereverzev, and O. Zolotukhin. Simulation studies on h-mode pedestal behavioru dur-ing type-i elms under various plasma conditions. In *Proceedings of the 28th EPS*

Conference on Controlled Fusion and Plasma Physics, Funchal, Portugal, pages 629–632, 2001.

[24] G. Valmorbida, M. Ahmadi, and A. Papachristodoulou. Stability analysis for a class of partial differential equations via semidefinite programming. *IEEE Transactions on Automatic Control*, 61(6):1649–1654, 2016.

[25] G. Valmorbida and A. Papachristodoulou. Introducing intsostools: A sostools plug-in for integral inequalities. In *Control Conference (ECC), 2015 European*, pages 1231–1236. IEEE, 2015.

[26] E. Witrant, E. Joffrin, S. Brémond, G. Giruzzi, D. Mazon, O. Barana, and P. Moreau. A control-oriented model of the current profile in tokamak plasma. *Plasma Physics and Controlled Fusion*, 49(7):1075, 2007.